# Supporting Information

## Teilum et al. 10.1073/pnas.0907387106

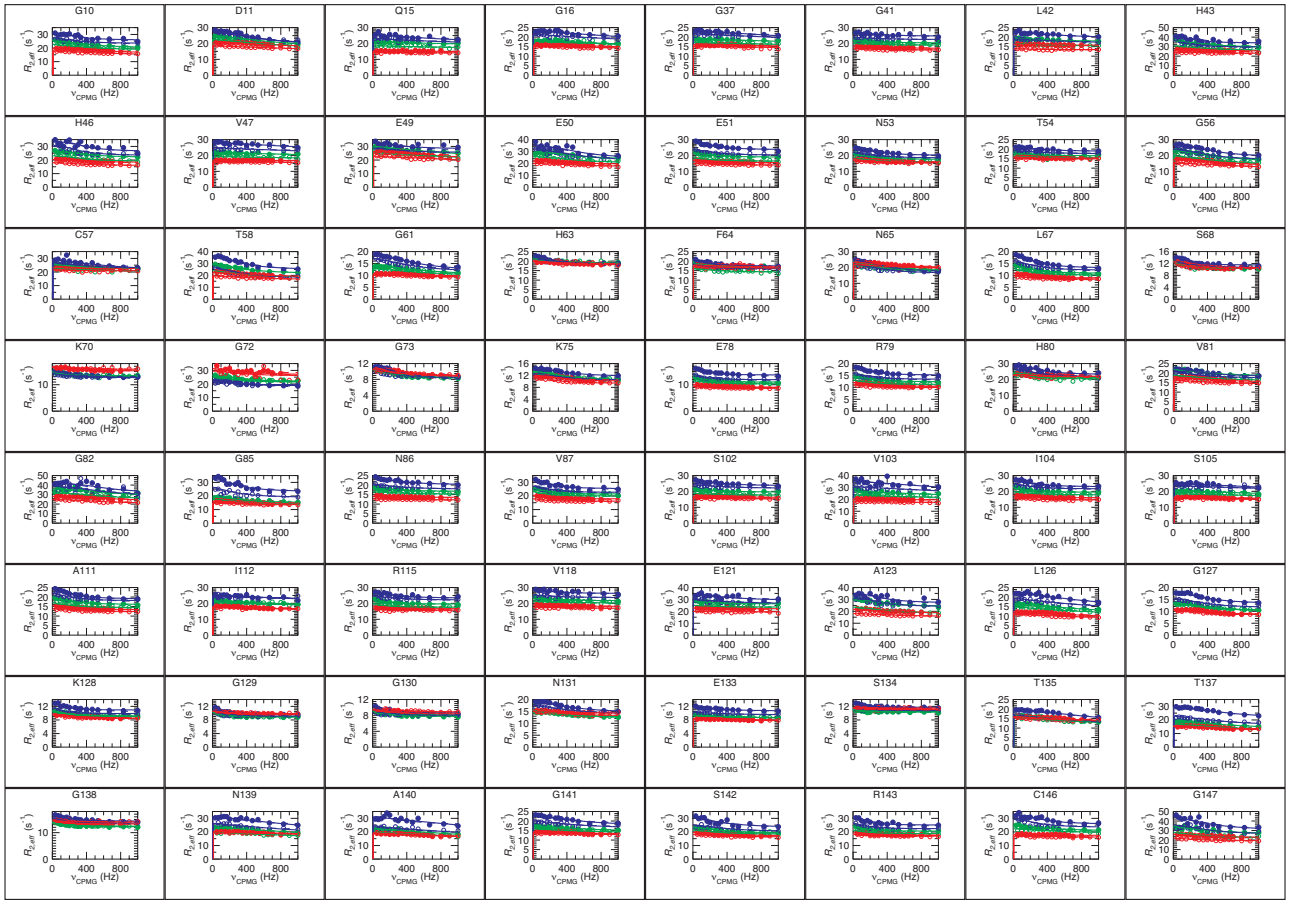


**Fig. S1.** $^{15}$N CPMG relaxation dispersion curves recorded at 2 static magnetic fields (open symbols, 500 MHz; filled symbols, 600 MHz) and 3 temperatures (blue, 18 °C; green, 25 °C; red, 32 °C) on WT apo-SOD1. The effective transverse relaxation rate ($R_{2,\mathrm{eff}}$) is plotted against the effective field strength ($\nu_{\mathrm{CPMG}}$) of the refocusing pulse train for datasets with significant dispersion ($P < .0005$). The solid lines represent a global fit with $k_{ex}$, $p_F$, and $\Delta H$ as global parameters. The optimized values for $k_{\mathrm{ex}}$ were $(2.3 \pm 0.2) \times 10^3$ s$^{-1}$ at 32 °C, $(2.2 \pm 0.1) \times 10^3$ s$^{-1}$ at 25 °C, and $(2.4 \pm 0.1) \times 10^3$ s$^{-1}$ at 18 °C.

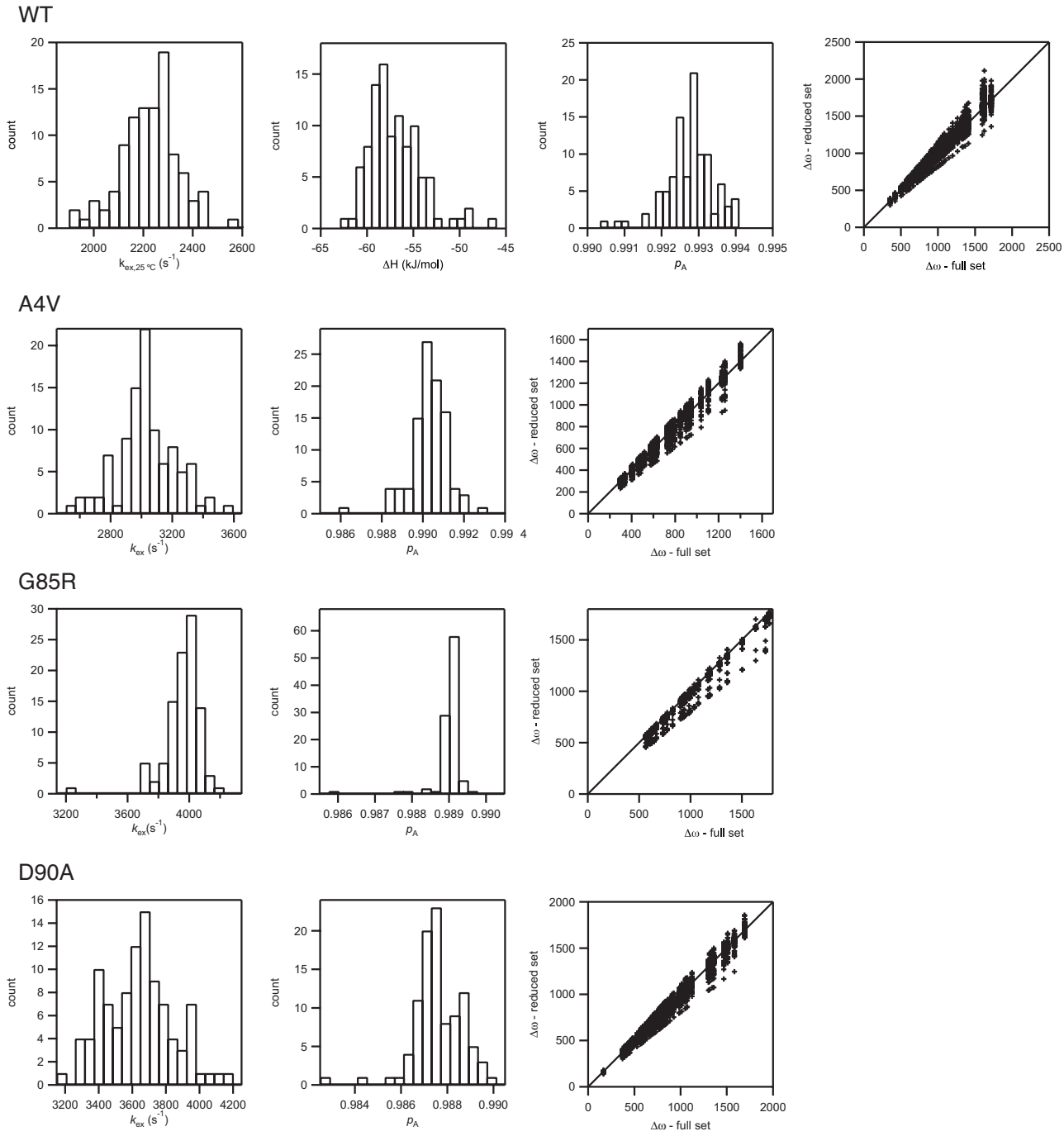


**Fig. S2.** Bootstrap analysis of the global fit routine. The robustness of the global fitting routine was assessed by global fits of 100 reduced datasets in which data for 20% of the residues included in the original global fit were randomly left out. The resulting distributions from the 100 fits for each variant show that the parameter distributions are centered around the optimized parameters obtained from the fits to the full datasets, and that no extreme outliers are observed.

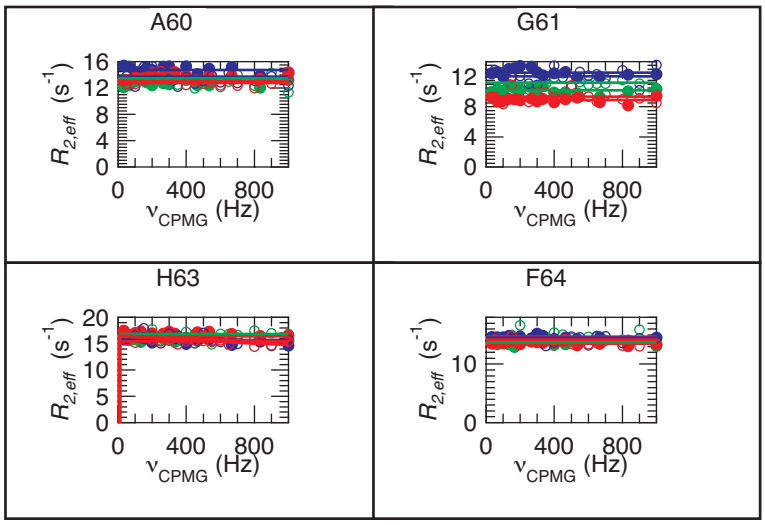


**Fig. S3.** $^{15}N$ CPMG relaxation dispersion curves for residues A60, G61, H63, and F64 in protein, where P62 is in the *cis* conformation. Symbols are as in Fig. S1.

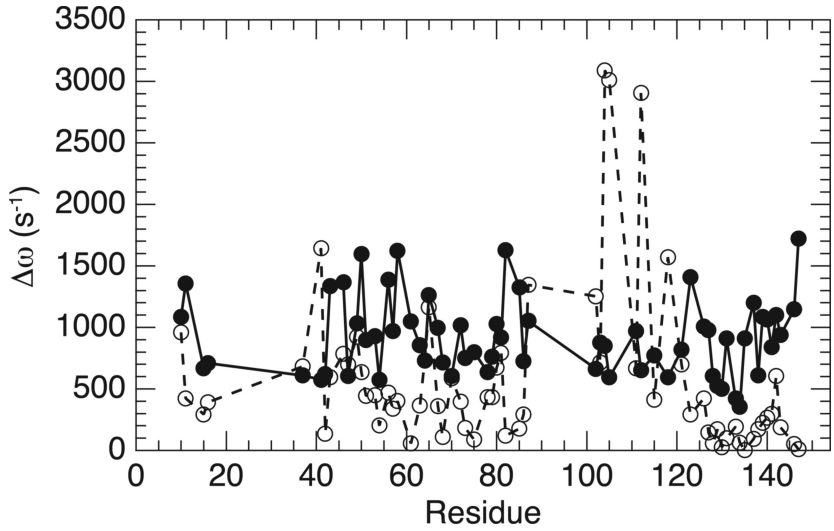


**Fig. S4.** Backbone amide $^{15}$N chemical shift differences in WT apo-SOD1 plotted versus residue number. The solid line and filled circles indicate $\Delta\omega_{FE}$ between the major and the minor states obtained from global fits of CPMG relaxation dispersions. The dashed line and open circles indicate the estimated change in chemical shift on unfolding, $\Delta\omega_{FU}$. In the regions that constitute loops IV and VII, $\Delta\omega_{FE}$ is larger than $\Delta\omega_{FU}$. Because $\Delta\omega_{FU}$ in these regions is small, the protein apparently becomes more structured in these loops in the minor state compared with the major state.

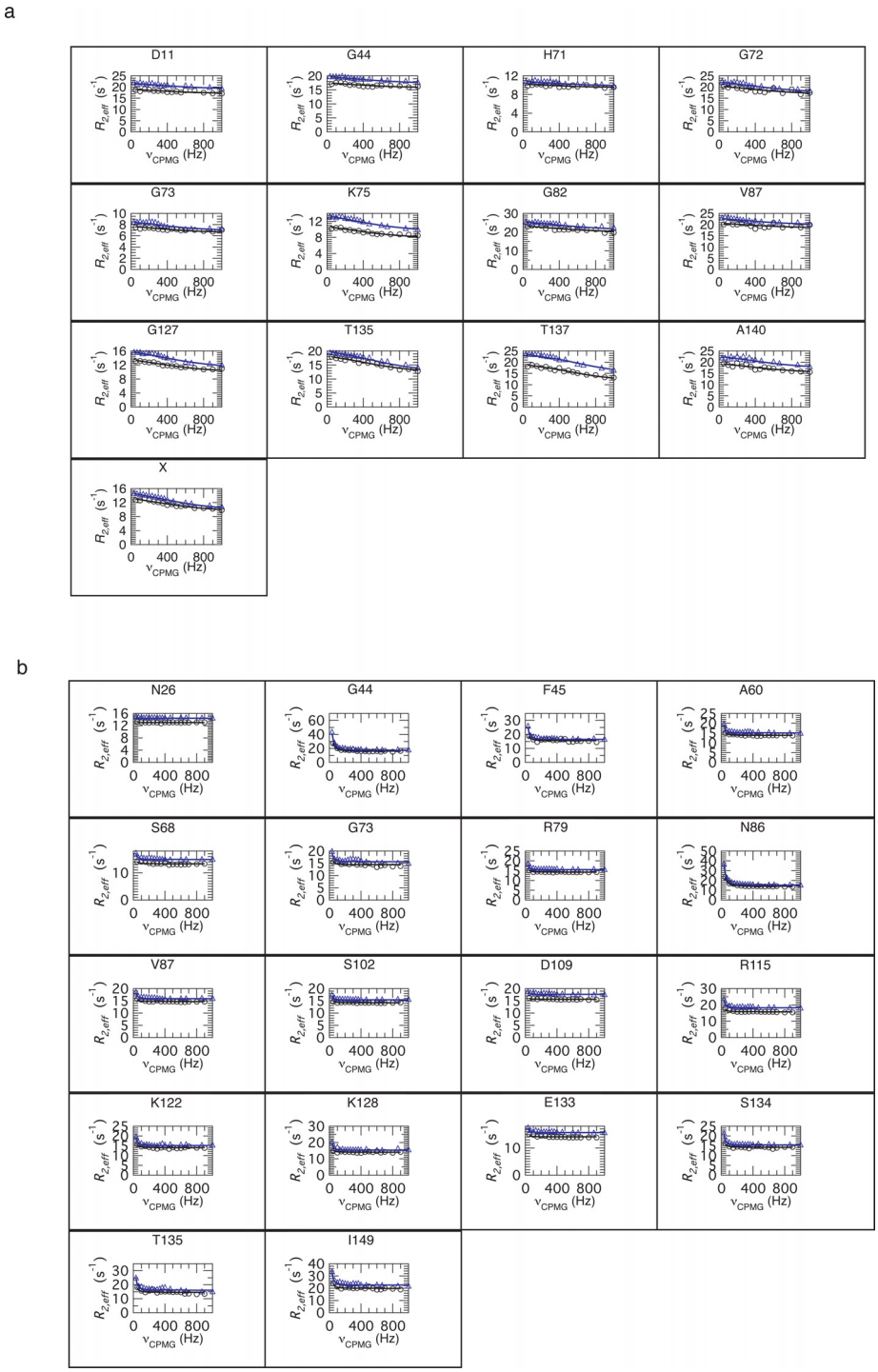


**Fig. S5.** $^{15}N$ CPMG relaxation dispersions. (*a*) Reduced WT apo-SOD1 at 2 static magnetic fields (black circles, 500 MHz; blue triangles, 600 MHz) at 25 °C. The effective transverse relaxation rate ($R_{2,eff}$) is plotted against the effective field strength ($\nu_{CPMG}$) of the refocusing pulse train for the 13 residues that show significant dispersions ($P < 0.01$). The ''X'' in the last panel indicates that the dataset could not be unambiguously assigned. The solid lines represent a global fit with optimized parameters, $k_{ex} = (3.4 \pm 0.3) \times 10^3\ s^{-1}$ and $p_E = 0.6\% \pm 0.1\%$. The exchange process is thus similar to that observed on disulfide oxidized apo-SOD1, although the exchange rate ($k_{ex}$) is faster. Due to the fast $k_{ex}$ combined with the low $p_E$, only the residues with the largest chemical shift differences between the exchanging states can be observed in the CPMG relaxation dispersion experiments. Therefore, only 13 residues show significant exchange in reduced apo-SOD1. (*b*) Zn-loaded WT SOD at 2 static magnetic fields (black circles, 500 MHz; blue triangles, 600 MHz) at 25 °C. The effective transverse relaxation rate ($R_{2,eff}$) is plotted against the effective field strength ($\nu_{CPMG}$) of the refocusing pulse train. The solid lines are a global fit to the equation for slow exchange, $R_{2,eff} = R_2 + k_A(1 - \sin(\Delta\omega\ \tau_{CPMG})/\Delta\omega\ \tau_{CPMG})$, for the 18 residues that were found to participate in the slow process. The optimized rate constant for the flux away from the observed state is $k_A = 22.4 \pm 0.7\ s^{-1}$. In addition, 14 residues show evidence of exchange, but these could not be quantified accurately because of the very small dispersion magnitudes.

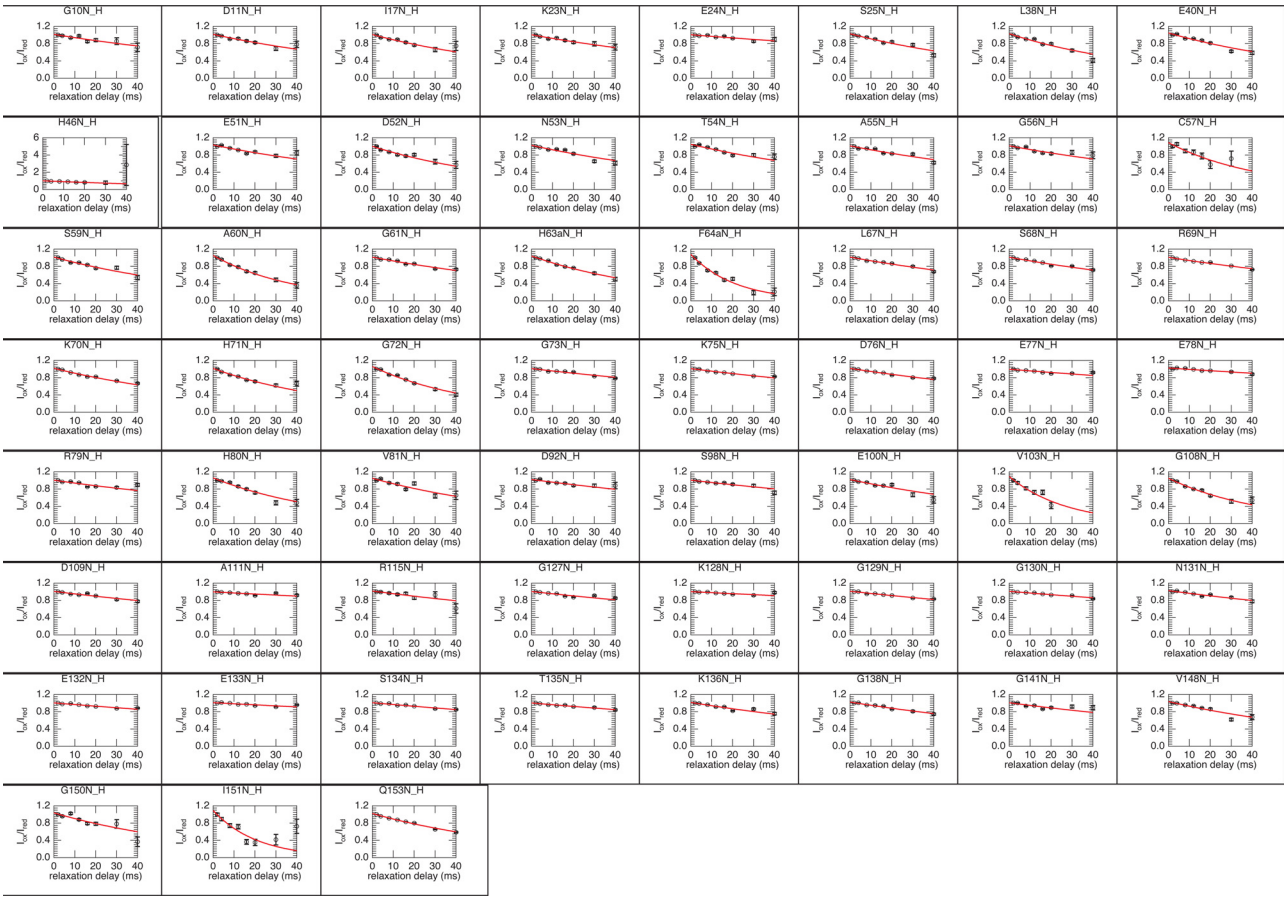


**Fig. S6.** Experimental data showing PRE decays. The relative cross-peak intensity ($I_{ox}/I_{red}$) is plotted against the relaxation delay. Only the 59 residues with data that fit an exponential decay significantly better ($P < 0.01$) than a constant value are shown. Because both $I_{ox}$ and $I_{red}$ decrease with relaxation delays, the data points at 30 and 40 ms generally are associated with large errors relative to the data points at shorter relaxation delays. Consequently, the data points at long relaxation delays weight less in the fit of the exponential decay.

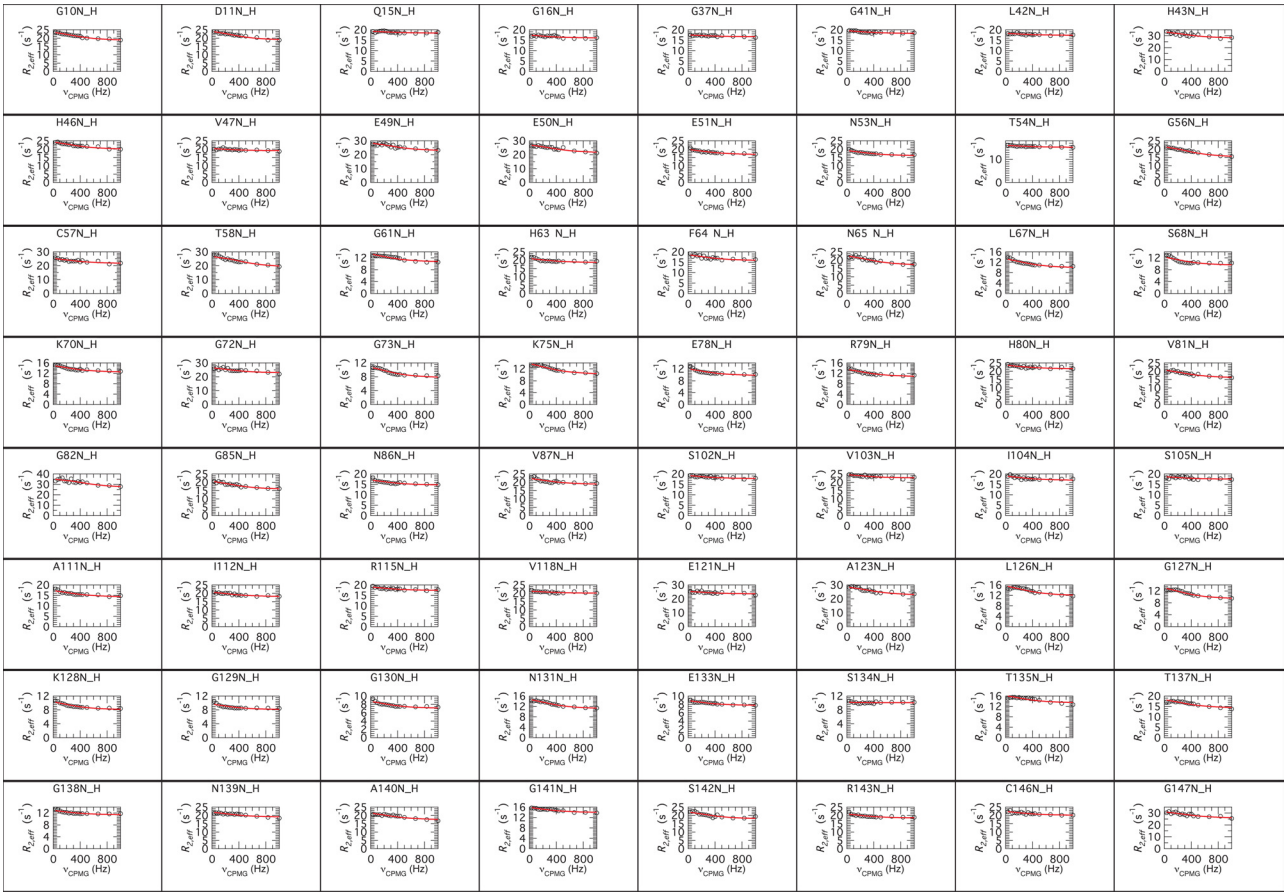


**Fig. S7.** Concentration dependence of the millisecond exchange process. $^{15}$N CPMG relaxation dispersion curves recorded at 600 MHz and 25 °C on 0.5 mM WT apo-SOD1. The solid lines represent a global fit of the experimental data. The optimized parameters for the exchange process are $p_E = 0.8\% \pm 0.1\%$ and $k_{ex} = (2.2 \pm 0.1) \times 10^3\ s^{-1}$.

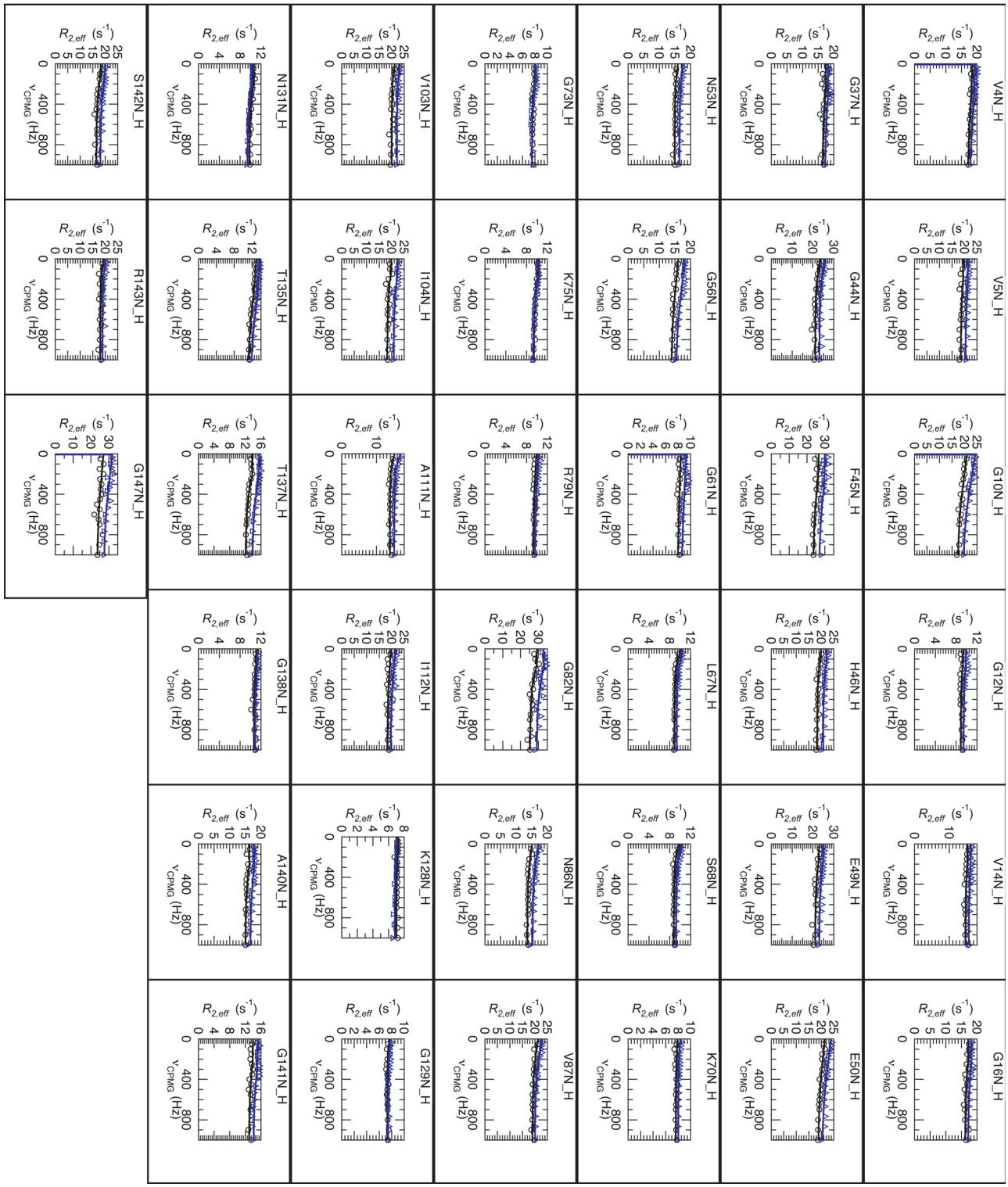


**Fig. S8.** $^{15}$N CPMG relaxation dispersion curves recorded on apo-SOD1 mutants A4V (*a*), G85R (*b*), and D90A (*c*) at 2 static magnetic fields (black circles, 500 MHz; blue triangles, 600 MHz) at 25 °C. The effective transverse relaxation rate ($R_{2,eff}$) is plotted against the effective field strength ($\nu_{CPMG}$) of the refocusing pulse train. Solid lines represent a global fit.

b

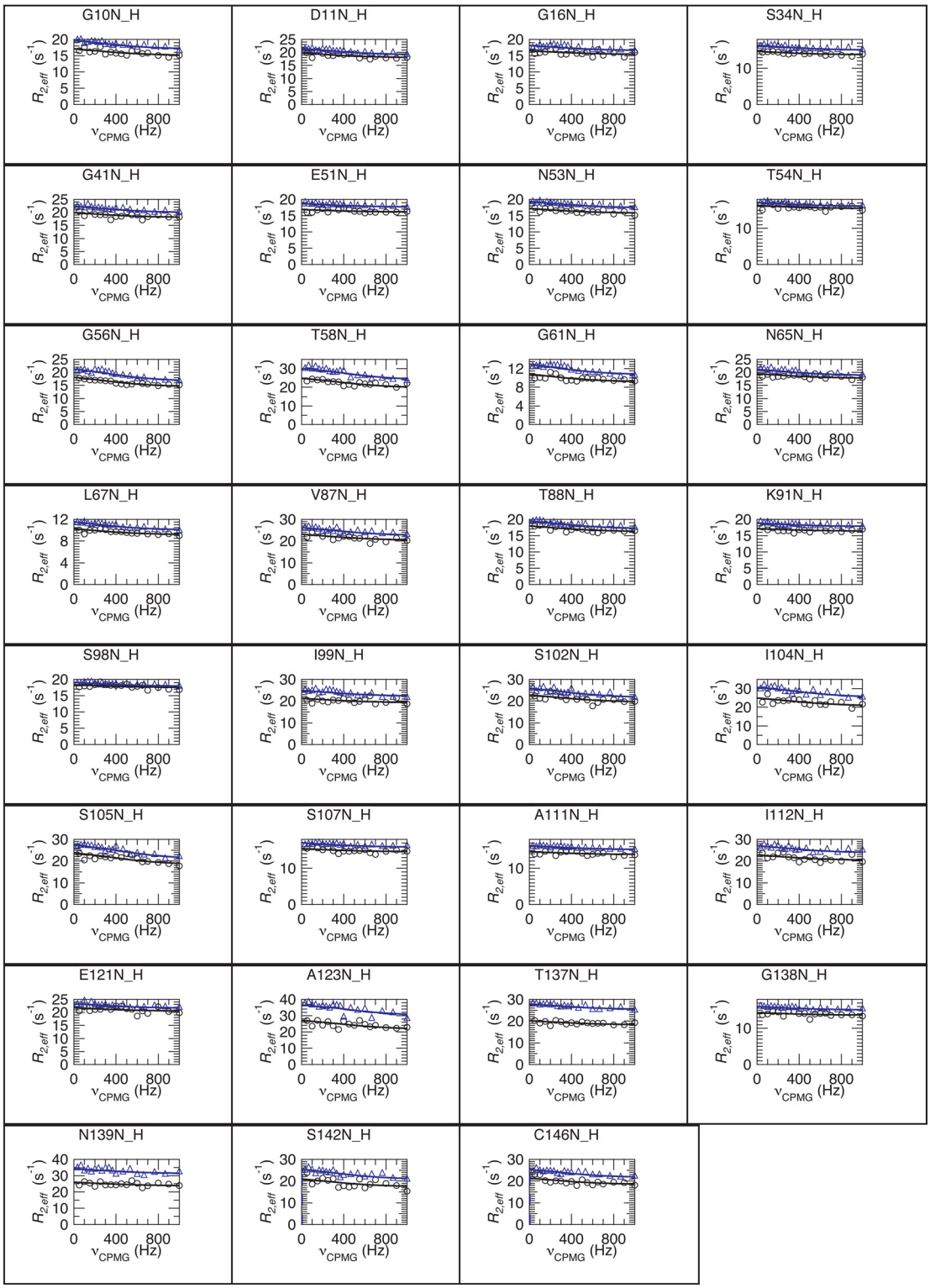


**Fig. S8.** Continued.

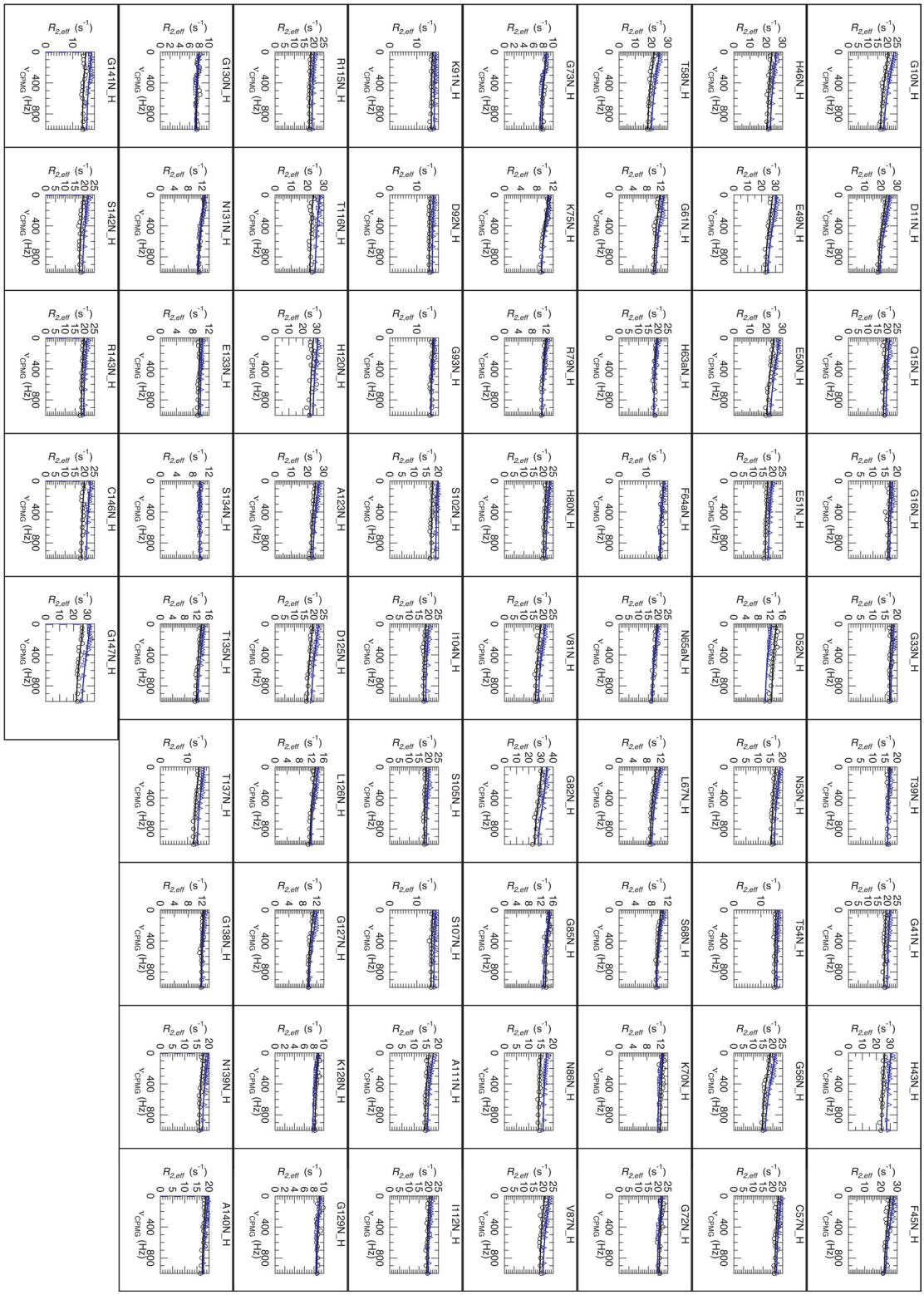


**Fig. S8.** Continued.

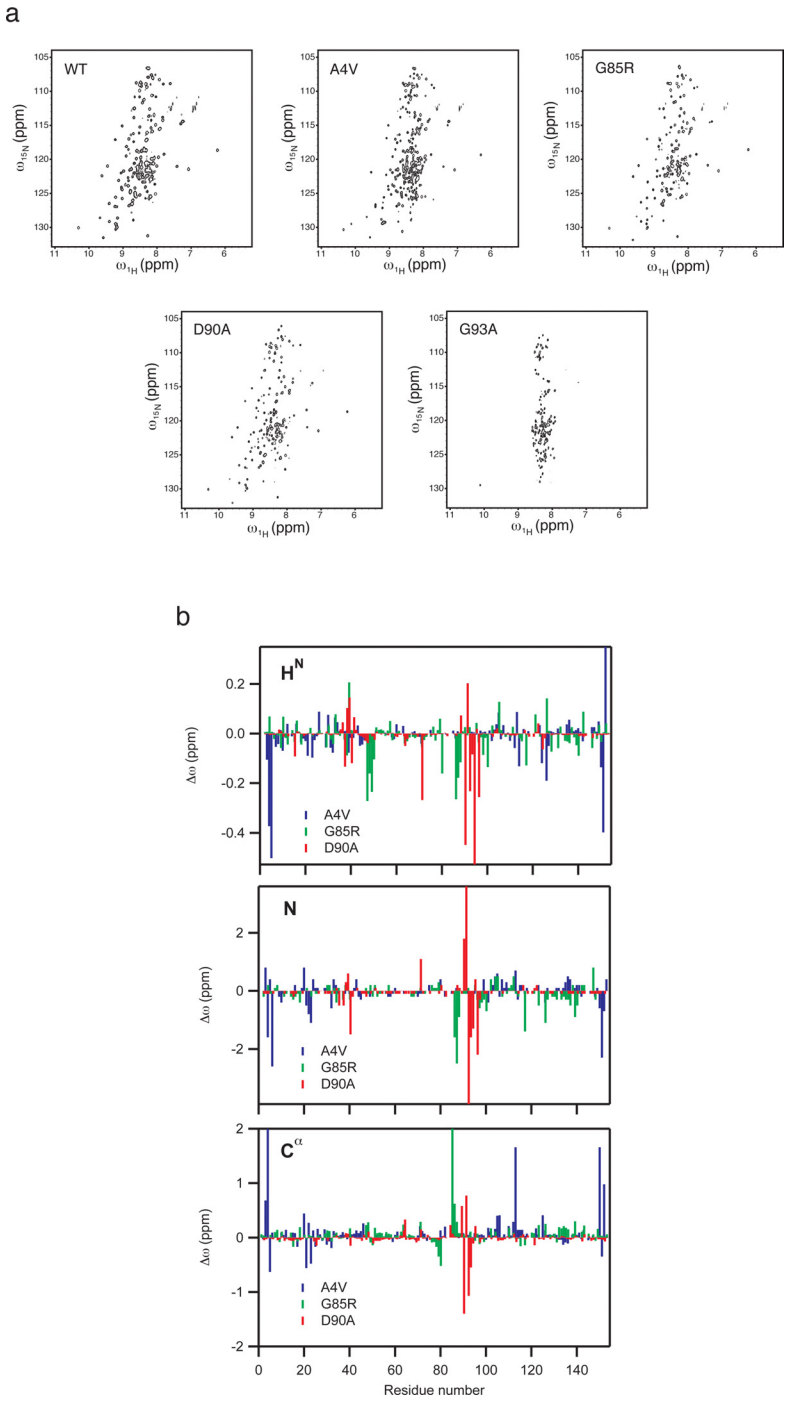


**Fig. S9.** NMR chemical shift analysis of apo-SOD WT and mutants in 10 mM MES, 1 mM EDTA, and 10% $D_2O$ (pH 6.3). (*a*) $^1H$,$^{15}N$-HSQC spectra of WT and mutant SOD. (*b*) Chemical shift differences ($^1H^N$, $^{15}N$, and $^{13}C^\alpha$) of the SOD1 mutants A4V, G85R, and D90A relative to the WT SOD1. For WT apo-SOD1, 142 out of the 148 nonproline $^1H^N$ and $^{15}N$ chemical shifts were assigned. Double sets of peaks were identified and assigned for 7 residues (60, 61, 63, 64, 65, 72, and 73) that are followed by prolines at positions 62, 66, and 74. In addition, chemical shifts were assigned for $^{13}C^\alpha$, $^{13}C^\beta$, and $^{13}C'$ in 150, 124, and 148 residues, respectively. From the chemical shift of P62 $C^\beta$, the double set of peaks around this residue can be assigned to a minor (≈25%) *cis* conformation and a major (≈75%) *trans* conformation. $C^\beta$ chemical shifts for the other proline residues were not assigned. For the D90A mutant, amide $^1H^N$ and $^{15}N$ chemical shifts were assigned for 141 residues, and for 5 of these, double sets of resonances were identified. In addition, $^{13}C^\alpha$ was assigned for 153 residues. For the A4V and G85R mutants, chemical shifts were assigned for fewer residues due to a greater extent of overlap in the HSQC spectra of these variants; see (*a*). ($^1H^N$, $^{15}N$)/$^{13}C^\alpha$/$^{13}C^\beta$/$^{13}C'$ chemical shifts were assigned for 130/143/116/143 and 126/143/119/144 residues in the A4V and G85R mutants, respectively. No double sets of resonances were assigned for these 2 mutants. All assignments have been deposited at the BioMagResBank; http://www.bmrb.wisc.edu (accession numbers: 15711, 15712, 15713, and 15714).

**Table S1. Data sizes and $\chi^2$ results for global fits**

| SOD variant | WT | A4V | G85R | D90A |
|---|---|---|---|---|
| Residues included | 64 | 39 | 31 | 68 |
| $N_{datapoints}$ | 6,144 | 1,404 | 1,116 | 2,312 |
| $N_{parameters}$ | 453 | 119 | 95 | 206 |
| $\chi^2$ | 3,557 | 312.1 | 641.3 | 520.2 |
| $\chi^2_{red}$ | 0.62 | 0.24 | 0.63 | 0.25 |

The global fit for WT includes data acquired at 3 different temperatures. The global fits for the mutants include data acquired at a single temperature.

**Table S2. Are $k_{ex}$ and $p_E$ different between mutants?**

| | WT and A4V | | WT and G85R | | WT and D90A | |
|---|---|---|---|---|---|---|
| Parameter tested | $k_{ex}$ | $p_E$ | $k_{ex}$ | $p_E$ | $k_{ex}$ | $p_E$ |
| F-ratio | 5.53 | 1.35 | 76.6 | 5.66 | 19.8 | 4.69 |
| *P* | 0.019 | 0.24 | $2.6710^{-18}$ | 0.017 | $8.8210^{-6}$ | 0.031 |

Dispersion data for WT apo-SOD1 were fit pairwise with data for the mutants, taking either $p_F$ or $k_{ex}$ as a parameter shared between WT and mutant. These fits were compared with fits in which $k_{ex}$ and $p_E$ were optimized as individual parameters for each variant. The model with a shared $k_{ex}$ (or $p_F$) and the model with individual $k_{ex}$ (or $p_F$) for WT and mutant are nested models, with the former being a simpler version of the latter ($k_{ex,wt} = k_{ex,mut}$ or $p_{F,wt} = p_{F,mut}$). The *F* test was used to test the hypothesis that $k_{ex}$ (or $p_F$) differs between WT and mutant against the null-hypothesis that $k_{ex}$ (or $p_F$) is the same for the 2 variants.